Interaction of IAPP and Insulin with Model Interfaces Studied Using Neutron Reflectometry

Christoph Jeworrek,[†] Oliver Hollmann,[†] Roland Steitz,[‡] Roland Winter,[†] and Claus Czeslik[†*]
[†]Fakultät Chemie, Technische Universität Dortmund, D-44221 Dortmund, Germany; and [‡]Helmholtz-Zentrum Berlin, D-14109 Berlin, Germany

ABSTRACT The islet amyloid polypeptide (IAPP) and insulin are coproduced by the β-cells of the pancreatic islets of Langerhans. Both peptides can interact with negatively charged lipid membranes. The positively charged islet amyloid polypeptide partially inserts into these membranes and subsequently forms amyloid fibrils. The amyloid fibril formation of insulin is also accelerated by the presence of negatively charged lipids, although insulin has a negative net charge at neutral pH-values. We used water-polymer model interfaces to differentiate between the hydrophobic and electrostatic interactions that can drive these peptides to adsorb at an interface. By applying neutron reflectometry, the scattering-length density profiles of IAPP and insulin, as adsorbed at three different water-polymer interfaces, were determined. The islet amyloid polypeptide most strongly adsorbed at a hydrophobic poly-(styrene) surface, whereas at a hydrophilic, negatively charged poly-(styrene sulfonate) interface, the degree of adsorption was reduced by 50%. Almost no IAPP adsorption was evident at this negatively charged interface when we added 100 mM NaCl. On the other hand, negatively charged insulin was most strongly attracted to a hydrophilic, negatively charged interface. Our results suggest that IAPP is strongly attracted to a hydrophobic surface, whereas the few positive charges of IAPP cannot warrant a permanent immobilization of IAPP at a hydrophilic, negatively charged surface at an ionic strength of 100 mM. Furthermore, the interfacial accumulation of insulin at a hydrophilic, negatively charged surface may represent a favorable precondition for nucleus formation and fibril formation.

INTRODUCTION

The islet amyloid polypeptide (IAPP) is a hormone that is synthesized by the β-cells of the pancreatic islets of Langerhans. Naturally, it is involved in controlling the level of glucose in the blood. On the other hand, it is the main component of amyloid deposits occurring with type 2 diabetes mellitus (1). The islet amyloid polypeptide is known to interact with negatively charged lipid membranes that contain, for instance, phosphatidylglycerol or phosphatidylserine lipids (2). This interaction was shown to accelerate amyloid fibril formation (3), and to trigger the permeabilization of lipid membranes (4). It was suggested that these two processes are independent of each other, i.e., membrane disruption can occur independent of the amyloid formation of IAPP (5). There is considerable experimental evidence that IAPP partially inserts into negatively charged lipid membranes (6,7), where transient α-helices are formed, before β-sheet and amyloid fibril formation set in (8). The islet amyloid polypeptide has 37 amino-acid residues and 3–4 positive charges at neutral pH-values. They are located on the N-terminal part of the polypeptide chain at positions 1 (Lys and α-C-NH_2), 11 (Arg), and 18 (His). These charges can bind favorably to negative charges of lipid headgroups. It was shown that the IAPP fragment of residues 1–19 inserts even better into a lipid membrane than full-length IAPP itself (6). As well as electrostatic interactions, once partially inserted, IAPP will certainly interact with lipid chains via hydrophobic interactions.

So far, little is known about the relative contributions of electrostatic and hydrophobic interactions to the binding of IAPP to negatively charged lipid membranes. Using lipid membranes as a binding substrate for IAPP, a clear separation of these two different kinds of interactions is virtually impossible. Therefore, in this study, the spontaneous adsorption of IAPP was characterized at model interfaces that were prepared by coating solid silicon substrates with different polymer films. A hydrophobic poly-(styrene) film can serve to assess the importance of hydrophobic interactions as a driving force for IAPP adsorption at an interface, whereas positively or negatively charged hydrophilic polyelectrolyte layers can mimic electrostatic charges of lipid headgroups. When these polymer surfaces are brought into contact with a highly diluted IAPP solution (1 μM), IAPP adsorbs spontaneously according to the strength of electrostatic or hydrophobic driving forces.

For comparison, a second peptide, insulin, was investigated in a similar way. Insulin is produced together with IAPP in the pancreatic β-cells. Insulin is a highly efficient inhibitor of IAPP amyloid fibrillation (9). Insulin does not form amyloid fibrils in vivo, but this process can be triggered easily in vitro by lowering the pH-value and raising the temperature (10,11), or by agitation in the presence of hydrophobic surfaces (12,13). These activating conditions represent a serious issue in the production and handling of insulin. A series of studies documented distinct aggregation pathways of insulin ending up in different amyloid fibril morphologies (14–17). It was also observed that the kinetics of insulin fibril formation at pH 7.4 and 60°C are significantly altered in the presence of lipid membranes, suggesting an insulin-lipid interaction

Submitted June 2, 2008, and accepted for publication November 5, 2008.

*Correspondence: claus.czeslik@uni-dortmund.de

Editor: Jill Trewhella.

0006-3495/09/02/1115/9 $2.00

doi: 10.1016/j.bpj.2008.11.006

(18). By adding the negatively charged lipid dioleoyl-*sn*-glycero-phosphatidylserine (DOPS) to a lipid membrane, the amyloid fibril formation of insulin could be accelerated. This represents a rather puzzling effect, because insulin has its isoelectric point at pH 5.3 (19), resulting in a negative net charge at pH 7.4 and a net electrostatic repulsion to DOPS lipid molecules. However, as will be shown here, a much stronger adsorption of insulin occurs at a negatively charged polyelectrolyte layer than at a positively charged one.

A series of techniques can be used to characterize protein adsorbates at aqueous-solid interfaces, such as attenuated total reflection-Fourier transform infrared (ATR-FTIR) spectroscopy, total internal reflection fluorescence (TIRF) spectroscopy, fluorescence microscopy, ellipsometry, and sum frequency generation (SFG) spectroscopy, among others (20). Whereas ATR-FTIR and TIRF spectroscopy are suitable for probing the secondary and tertiary structures of adsorbed protein molecules, ellipsometry allows for a determination of the adsorbed mass with a high time resolution. Applying SFG spectroscopy, the alignment of protein residues may be detected. Here, the interaction of IAPP and insulin with various polymer surfaces was quantified, using neutron reflectometry (21). This method is particularly suitable for probing the density profile of protein adsorbates at aqueous-polymer interfaces for several reasons (22–24). By using D_2O as the solvent, a high contrast to the polymer film and the adsorbed protein can be generated. When the protein adsorbs on a polymer film, ultrasensitive detection of very thin protein adsorbates in the Å-region is possible, which is important when studying small peptides such as IAPP. Furthermore, due to its low energy, a neutron beam does not cause any damage to biological samples, as may be the case using x-rays, for example.

MATERIALS AND METHODS

Peptide solutions

Human IAPP was purchased from EMD Biosciences (La Jolla, CA). All other chemicals were from Sigma-Aldrich (Taufkirchen, Germany). We dissolved 0.5 mg of IAPP in 1 mL of 2,2,2-trifluoroethanol, and we dried 128 μL of this solution on the inner side of a round-bottom flask, using a gentle stream of nitrogen. Then we added 16 mL of buffer solution to obtain an IAPP sample solution with a concentration of 1 μM. The buffer solution contained 10 mM N-morpholinopropanesulfonic acid (MOPS) in D_2O, and was adjusted to pD 7.4 by adding NaOH (pD = pH-meter reading + 0.4 (25)). An IAPP solution was used immediately after preparation for neutron reflectometry. Bovine insulin was purchased from Sigma (catalog No. I5500, Sigma, St. Louis, MO). An insulin stock solution was prepared in D_2O (pD 2.3) at a concentration of 1 mg/mL. Insulin sample solutions (0.1 mg/mL = 17 μM) were prepared by tenfold dilution of the stock solution, using D_2O-buffer solutions adjusted to pD 7.4 or 2.3.

Polymer surface coating

Silicon wafers were purchased from Siliciumbearbeitung Andrea Holm (Tann, Germany). They were of an 8 × 5 × 1.5 cm size, and the two large sides were polished. The wafers were cleaned in a 1:1:4 mixture of NH_3 (30%), H_2O_2 (30%), and H_2O, followed by intensive rinsing with pure water (modified Radio Corporation of America cleaning procedure (26)). Perdeuterated poly-(styrene) (dPS, Fig. 1) was purchased from Polymer Standards Service (Mainz, Germany). A dPS film on a silicon wafer was prepared by depositing a 6-mg/mL dPS solution in toluene on one of the large, polished sides of the silicon wafer. Then the silicon wafer was spun at 4500 rpm for 1 min (spin-coater KW-4A from Chemat Technology, Northridge, CA). The polyelectrolytes poly-(ethylene imine) (PEI, molar mass = 750,000 g mol^{-1}, Fig. 1), poly-(styrene sulfonate) (PSS, molar mass = 70,000 g mol^{-1}, Fig. 1), and poly-(allylamine hydrochloride) (PAH, molar mass = 70,000 g mol^{-1}, Fig. 1) were obtained from Sigma. A polyelectrolyte multilayer was built up on a silicon wafer by the following steps (27): initial immersion of the wafer into a PEI aqueous solution (0.01 mol/L monomers) for 20 min, alternate immersion into PSS and PAH aqueous solutions (0.01 mol/L monomers, 1 mol/L sodium chloride) for 20 min, and intensive rinsing with pure water after each polyelectrolyte deposition step. All polymer films were attached to a silicon block via noncovalent bonds, such as electrostatic and hydrophobic interactions.

Neutron reflectometry

Neutron reflectivity measurements were performed at the Helmholtz-Zentrum Berlin (Berlin, Germany), using the instrument V6 (28). The neutron wavelength selected by a graphite monochromator was 4.66 Å. Higher-order wavelengths were suppressed by a Be filter cooled with liquid nitrogen. The sample cell consisted of a silicon wafer coated with a polymer film on the bottom surface (8 × 5 cm) and a Teflon trough, which was fixed underneath and filled with the sample solution. The sample cell was heated using a thermostating water jacket. Neutrons entered the silicon wafer through one of the small sides, were reflected in part at the silicon-solution interface, and left the silicon wafer through the other small side. Neutron reflectivities were recorded with a fixed incident neutron beam in $\theta/2\theta$ geometry, using a ^{3}He detector. Reflected intensities were normalized to the number of incoming neutrons hitting the silicon-solution interface, which yields the neutron reflectivity, and were scaled as a function of wavevector transfer, $Q = (4\pi/\lambda) \sin\theta$ (λ is the neutron wavelength, and θ is the angle of incidence), where θ ranges from 0° to ~2.5°. Before each run, the sample cell was rinsed and filled with freshly prepared sample solution, and was equilibrated for at least 1 h.

RESULTS AND DISCUSSION

IAPP adsorption at polymer-water interfaces

Neutron reflectivities of water-polymer interfaces were collected at pD 7.4 and 23°C in the absence and presence of dissolved IAPP (1 μM). To check for electrostatic

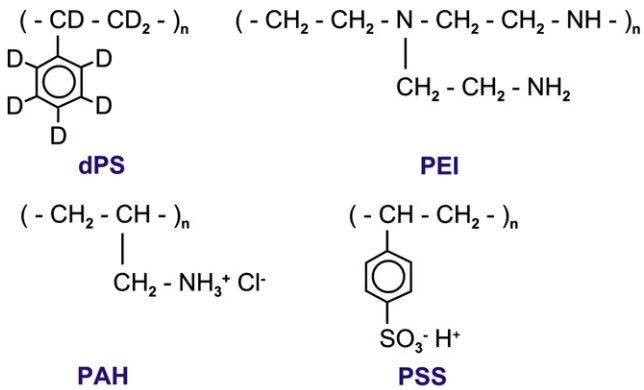

FIGURE 1 Chemical structures of polymers used in this study.

interactions, additional neutron reflectivities were measured after adding 100 mM NaCl. Because it was reported that the adsorption, rearrangement, and relaxation of IAPP at lipid monolayers may take several hours (8), neutron reflectivity curves of samples containing IAPP were measured after 8 h of incubation (Fig. 2). These curves are characterized by pronounced oscillations reflecting a high scattering-length density contrast between the interfacial structures and the sample solutions. All data were analyzed by fitting calculated curves as based on layer models for interfacial structures.

The following results were obtained on a hydrophobic dPS surface. A first neutron reflectivity curve was measured when the dPS film was in contact with a 3:1 D_2O/H_2O mixture as a sample solution in the absence of IAPP (data not shown). This sample solution has a different scattering-length density than dPS, so that the thickness and roughness of the dPS film on the silicon wafer can be determined precisely. The obtained neutron reflectivity curve can be analyzed, assuming the one-layer model Si/dPS/solution. In the fitting process, the scattering-length densities of the three components were fixed to 2.07×10^{-6} Å^{-2} (Si), 6.2×10^{-6} Å^{-2} (dPS), and 4.6×10^{-6} Å^{-2} (D_2O/H_2O) (21,29), whereas the dPS thickness and the two roughness values for both sides of the dPS film were varied. The obtained scattering-length density profile is plotted in Fig. 3, and the fitting parameters are listed in Table 1. A depletion layer is likely to be formed at the dPS-solution interface in the absence of a peptide (30). This depletion layer has a scattering length density of ~5.7×10^{-6} Å^{-2}, and thus merges into the dPS-solution interfacial roughness. In the next step, the D_2O/H_2O mixture was exchanged by a 1-μM IAPP solution in D_2O, leading to the formation of an IAPP

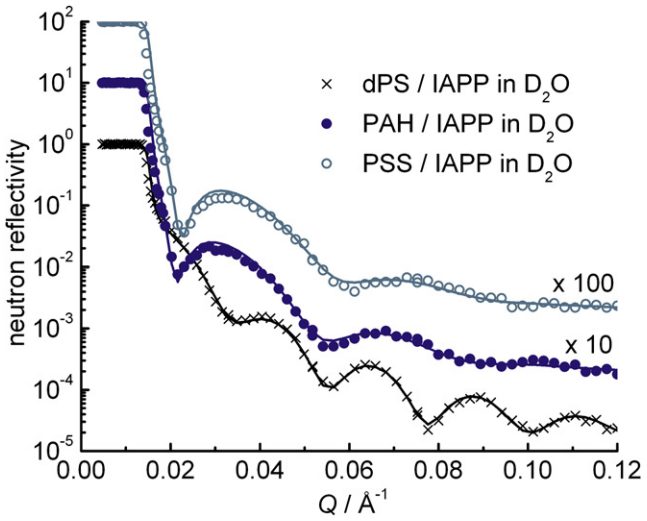

FIGURE 2 Neutron reflectivity curves of silicon-polymer-solution interfaces with adsorbed IAPP (pD 7.4, 23°C, 8 h of incubation, no added NaCl). Polymer films are composed of dPS, a polyelectrolyte multilayer ending with PAH, and a polyelectrolyte multilayer ending with PSS. Fits are shown as solid lines. The PAH and PSS data are shifted vertically for clarity.

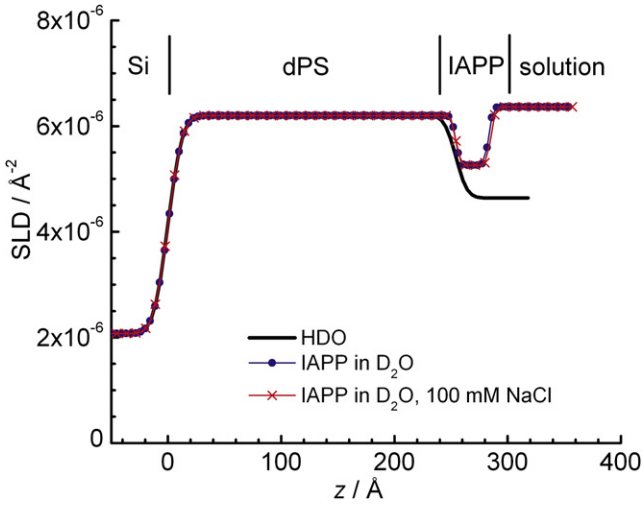

FIGURE 3 Scattering-length density (SLD) profiles of a silicon-dPS-solution interface without and with adsorbed IAPP, as derived from neutron reflectivity curves. Thick solid curve was obtained with a 3:1 D_2O/H_2O mixture (denoted as HDO) in the absence of IAPP. Thin solid lines with symbols reflect interfacial structures when the solution contains 1 μM IAPP in D_2O (pD 7.4, 23°C). In the latter case, an IAPP adsorbate forms on the dPS surface.

adsorbate on the dPS surface. Because dPS and D_2O have approximately the same scattering-length density, the IAPP adsorbate has a high contrast to both the polymer and the solution. After 8 h of incubation, a neutron reflectivity curve was measured (Fig. 2), which could be analyzed on the basis of the two-layer model Si/dPS/IAPP adsorbate/IAPP solution (Table 1). The corresponding scattering-length density profile is plotted in Fig. 3.

As seen in Fig. 3, IAPP forms a relatively thick protein adsorbate (thickness $d = 29$ Å) that extends over the diffuse dPS-solution interface. In the presence of IAPP, the formation of a depletion layer at the dPS-solution interface is not expected to occur. The amphiphilic nature of the peptide prohibits this phenomenon by accumulating at this interface. The scattering-length density of the IAPP adsorbate may be represented as:

$$\rho_{\text{adsorbate}} = \phi_{\text{protein}}\rho_{\text{protein}} + \left(1 - \phi_{\text{protein}}\right)\rho_{\text{solution}} \quad (1)$$

where ϕ_{protein} is the volume fraction of IAPP molecules in the adsorbate, ρ_{protein} is the scattering-length density of an IAPP molecule, and ρ_{solution} is the scattering length density of the solution. For IAPP, ρ_{protein} was calculated as 3.56×10^{-6} Å^{-2}, using the primary sequence of IAPP (31), neutron scattering lengths published by the National Institute of Standards and Technology (29), and a specific volume of $v = 0.72$ cm^3 g^{-1} (corresponding to a molecular volume of 4680 Å^3 (7)). The ρ_{solution} is essentially given by the scattering-length density of D_2O (6.4×10^{-6} Å^{-2}), and $\rho_{\text{adsorbate}}$ is the scattering-length density of the IAPP adsorbate as shown in Fig. 3 (5.3×10^{-6} Å^{-2}). Then the volume fraction of IAPP in the adsorbate on a dPS film can be calculated

TABLE 1 Fitting parameters and adsorbed amounts of IAPP and insulin at different polymer surfaces under various conditions

	T/°C	pD	c_{NaCl}/mM	$\rho_{pol}/10^{-6}$ Å^{-2}	d_{pol}/Å	σ_{pol}/Å	$\rho_{ads}/10^{-6}$ Å^{-2}	d_{ads}/Å	σ_{ads}/Å	Γ/mg m^{-2}
dPS				6.2	254	8				
dPS/IAPP	23	7.4	0	6.2	254	3	5.3	29	3	1.6
dPS/IAPP	23	7.4	100	6.2	254	3	5.3	31	3	1.7
PAH*				4.8	173	19				
PAH/IAPP‡	23	7.4	0	4.8	177	20				0.3
PAH/IAPP‡	23	7.4	100	4.8	178	20				0.4
PSS†				4.7	154	22				
PSS/IAPP‡	23	7.4	0	4.7	163	23				0.8
PSS/IAPP‡	23	7.4	100	4.7	156	23				0.2
dPS				6.2	219	18				
dPS/insulin	20	7.4	0	6.2	213	3	5.7	55	3	1.7
dPS/insulin	20	2.3	100	6.2	200	3	5.7	59	3	1.7
dPS/insulin	60	2.3	100	6.2	200	3	5.7	62	3	1.8
PAH*				4.5	263	8				
PAH/insulin	20	7.4	0	4.5	263	5	4.8	19	5	1.3
PAH/insulin	20	7.4	100	4.5	263	5	5.0	16	5	1.0
PSS†				4.3	296	9				
PSS/insulin	20	7.4	0	4.3	296	5	4.5	30	5	2.5
PSS/insulin	20	7.4	100	4.3	296	5	4.5	34	5	2.9
PSS/insulin	60	7.4	100	4.3	296	5	4.9	23	5	1.6

The IAPP concentration in solution was 1 μM, the insulin concentration was 0.1 mg mL^{-1} (17 μM), and ρ_{pol}, d_{pol}, σ_{pol}, ρ_{ads}, d_{ads}, σ_{ads} represent scattering-length density, thickness, and roughness of the polymer and adsorbate layers, respectively. The experimental error for the adsorbed amount, Γ, was estimated as ± 0.2 mg m^{-2}.

*Polyelectrolyte multilayer ending with PAH.

†Polyelectrolyte multilayer ending with PSS.

‡Polyelectrolyte multilayer and IAPP are modeled as single layer.

from Eq. 1 as $\phi_{protein} = 0.39$. The adsorbed mass of IAPP per interfacial area is then given as:

$$\Gamma = \frac{\phi_{protein} d}{v}. \quad (2)$$

With $\phi_{protein} = 0.39$, $d = 29$ Å, and $v = 0.72$ cm^3 g^{-1}, one obtains $\Gamma = 1.6$ mg m^{-2}. This value is at the lower limit of adsorbed amounts found for proteins. For example, $\Gamma = 1.8$ mg m^{-2} for lysozyme (32), and $\Gamma = 2.7$ mg m^{-2} for RNase A (33), at a silica-water interface. Assuming hypothetical spherical folding, IAPP would have a diameter of ~20 Å. A two-dimensional hexagonal packing of spherical IAPP molecules would yield a monolayer coverage of 1.9 mg m^{-2}. When IAPP adopts a nonfolded, open conformation, the monolayer capacity is likely to be smaller than this theoretical value, in reasonable agreement with the observed amount of 1.6 mg m^{-2}. Indeed, the conformation of IAPP in solution is largely unordered (34). However, IAPP molecules are not arranged side-by-side on a rough dPS surface, as can be judged from the adsorbate thickness (29 Å), which is larger than a hypothetical IAPP diameter (20 Å).

An additional neutron reflectivity curve was measured 8 h after rinsing the sample cell with a 1-μM IAPP solution containing 100 mM NaCl (data not shown). The corresponding scattering-length density profile essentially overlaps that measured without salt (Fig. 3). This result is consistent with a pure hydrophobic interaction between IAPP and dPS, and a lack of any slow rearrangements of IAPP molecules at the hydrophobic dPS surface on a time scale of hours.

To probe the electrostatic driving forces of IAPP adsorption, polyelectrolyte multilayers were built up on a silicon wafer. The structures of the multilayers are given as Si-PEI-PSS-(PAH-PSS)$_2$-PAH and Si-PEI-PSS-(PAH-PSS)$_2$. They are terminated with either positively charged PAH or negatively charged PSS. In both cases, a first neutron reflectivity curve was measured with D_2O-buffer solution without IAPP, to determine the scattering-length density, the thickness, and the roughness of each polyelectrolyte multilayer (Table 1). The corresponding scattering-length density profiles are shown in Fig. 4. The IAPP was then adsorbed at these polymer films by filling the sample cell with a 1-μM IAPP solution. Neutron reflectivity curves were measured after 8 h of incubation (Fig. 2). In the fitting analysis of these data, a one-layer model Si/multilayer/solution could be used. Adsorbed IAPP could be modeled simply by increasing the thickness of the multilayer. No additional layer had to be assigned to adsorbed IAPP (Table 1). Because the scattering-length densities of an IAPP adsorbate (Fig. 3) and a polyelectrolyte multilayer (Fig. 4) are similar, this simplification is a reasonable approach. The obtained scattering-length density profiles are also plotted in Fig. 4.

On a polyelectrolyte multilayer ending with positively charged PAH, only very small amounts of IAPP are adsorbed. The film thickness increases from 173 to 177 Å only (Table 1), i.e., just beyond the experimental error of this parameter (~3 Å). The change in scattering-length density profile upon addition of IAPP to the solution after 8 h of incubation (Fig. 4) yields an IAPP surface

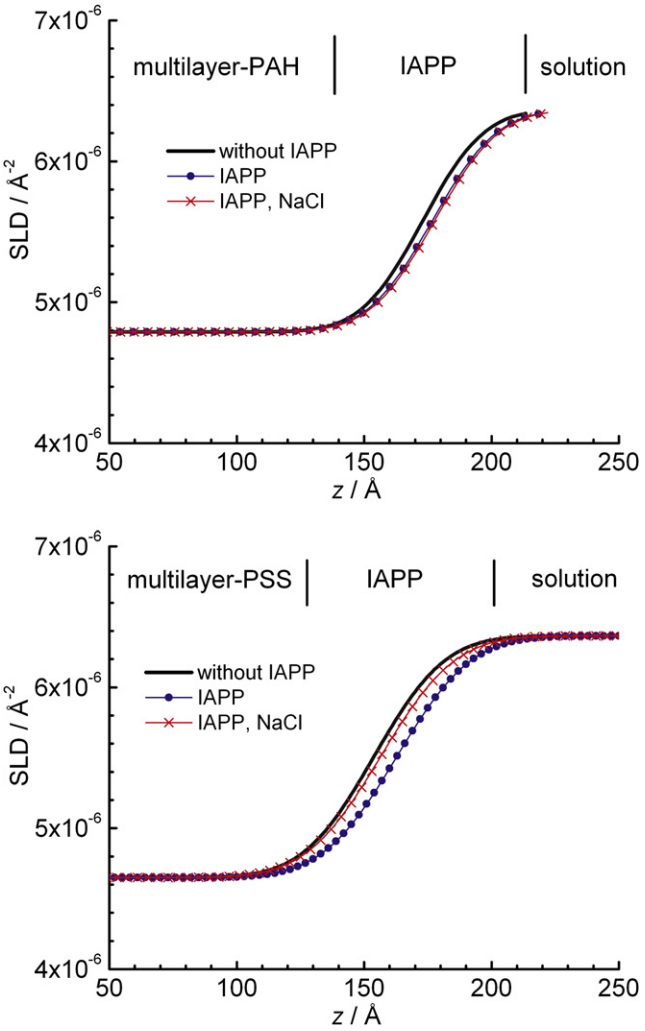

FIGURE 4 Scattering-length density (SLD) profiles of silicon-polyelectrolyte multilayer-solution interfaces. Thick solid curves indicate interfacial structures in the absence of IAPP. Thin solid curves with symbols reflect interfacial structures when the solution contains 1 μM IAPP. The concentration of NaCl (if added according to legends) is 100 mM. The silicon surface is located at $z = 0$ Å.

concentration of 0.3 mg m^{-2} (calculation according to Eqs. 1 and 2). This low surface concentration is a result of electrostatic repulsion, because both PAH and IAPP carry positive charges only. However, some weak hydrophobic interaction might be responsible for the small amount of IAPP adsorbed at the PAH layer. The degree of adsorption could not be changed by adding salt to the peptide solution: The scattering-length density profile measured after 8 h of incubation with 1 μM IAPP and 100 mM NaCl essentially overlaps with that measured previously, in the absence of salt (Fig. 4). Adding salt will certainly shield the repulsive electrostatic interactions between PAH and IAPP. However, a major attractive interaction is still missing.

In the case of a polyelectrolyte multilayer ending with PSS, significantly more IAPP adsorbs. After 8 h of incubation with a 1-μM IAPP solution, the adsorbed amount is 0.8 mg m^{-2}, as calculated from the scattering-length density profiles shown in Fig. 4 using Eqs. 1 and 2. Because PSS is negatively charged, there is an attractive electrostatic driving force for IAPP to adsorb at this polyelectrolyte. Indeed, when adding 100 mM NaCl to the IAPP solution, most of the adsorbed IAPP desorbs from the PSS layer. A residual amount of only 0.2 mg m^{-2} remains (Fig. 4), comparable to that determined at the PAH layer where no attractive electrostatic interactions exist.

Remarkably, the adsorbed amount of 0.8 mg m^{-2} of IAPP, as observed at the negatively charged PSS layer, is much less than that found at the hydrophobic dPS film (1.6 mg m^{-2}; see above). It is important to note that dPS and PSS, as used in this study, have a similar molecular structure. The PSS contains additional sulfate groups only (and is not perdeuterated). The surface roughness of PSS is slightly higher (Figs. 3 and 4). Therefore, one may conclude that IAPP can interact with an interface via hydrophobic interactions much stronger than via electrostatic attraction. This conclusion may shed some light on the binding mechanism of IAPP at negatively charged lipid membranes. If there were only attractive electrostatic interactions between IAPP and the lipid headgroups, IAPP would only touch the membrane surface and readily unbind, especially at the physiological salt concentration of 150 mM. However, the attractive electrostatic interactions might reduce the energy barrier for IAPP to penetrate into the lipid chain region. This process involves a separation of neighboring lipid molecules, which might be facilitated by IAPP electrostatically bound to the lipid headgroups. Finally, strong and permanent binding of IAPP at the membrane seems to be achieved through hydrophobic interactions with the lipid chains only.

Insulin adsorption at polymer-water interfaces

For comparison, the adsorption of insulin was also studied at a hydrophobic dPS, a positively charged PAH, and a negatively charged PSS surface, using neutron reflectometry. Fig. 5, depicts selected neutron reflectivity curves. In the case of the hydrophobic dPS surface, a first neutron reflectivity curve was measured using a 3:1 D_2O/H_2O mixture in the absence of insulin (denoted as HDO in Fig. 5). This solvent has a significantly lower scattering-length density than the dPS film, so that the film thickness and roughness can be determined precisely. Applying the one-layer model Si/dPS/HDO, the experimental neutron reflectivity curve was fitted (Fig. 5). The obtained scattering-length density profile indicates a dPS film thickness of 219 Å, and a dPS-solution interfacial roughness of 18 Å (Fig. 6, Table 1). Then the sample cell was filled with an insulin solution in D_2O (pD 7.4). In this case, an insulin adsorbate forms on the dPS surface. The corresponding neutron reflectivity curve was therefore fitted with a two-layer model Si/dPS/insulin adsorbate/insulin solution (Fig. 5 and Table 1). The corresponding scattering-length density profile is shown in Fig. 6. The dPS film

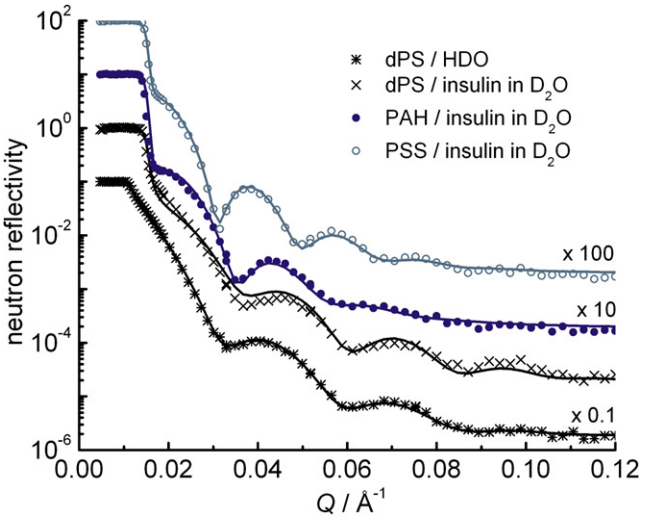

FIGURE 5 Neutron reflectivity curves of silicon-polymer-solution interfaces without and with adsorbed insulin (pD 7.4, 20°C, 1 h of incubation). Symbols indicate experimental data. Fits are shown as solid lines. Curves are shifted vertically for clarity.

thickness is apparently smaller in the presence of an insulin adsorbate (213 Å, Table 1). This can be explained by the relatively great roughness of the dPS film surface. When insulin adsorbs, it partially penetrates into this rough interface (Fig. 6). As a result, the observed thickness of 213 Å can no longer be regarded as a true value, but merely as the distance from the Si surface where the insulin adsorbate is located.

From the scattering-length density profile of a dPS surface in contact with an insulin solution at pD 7.4 (Fig. 6), a thickness of $d = 55$ Å and a scattering length density $\rho_{\text{adsorbate}} = 5.67 \times 10^{-6}$ Å^{-2} can be deduced for the insulin adsorbate. The scattering-length density of insulin in D_2O was found to be $\rho_{\text{protein}} = 3.27 \times 10^{-6}$ Å^{-2}, using the primary sequence of insulin (35), neutron-scattering lengths published by the National Institute of Standards and Technology (29), and a specific volume of $v = 0.717$ cm^3 g^{-1} (36). With $\rho_{\text{solution}} = 6.4 \times 10^{-6}$ Å^{-2}, the volume fraction of insulin in the adsorbate on a dPS film can be calculated from Eq. 1 as $\phi_{\text{protein}} = 0.23$. Then Eq. 2 yields an adsorbed mass of 1.7 mg m^{-2} on a dPS surface. However, the fit of the neutron reflectivity curve obtained with insulin adsorbed on a dPS surface shows small systematic deviations (Fig. 5). This finding suggests broad lateral inhomogeneities of the insulin adsorbate. In a neutron reflectivity experiment, the interfacial structure is laterally averaged on the length scale of micrometers (21), whereas in our experiments, the total area probed by the neutron beam was ~20 cm^2. If the interfacial roughness has a waviness on a scale of more than micrometers, the measured neutron reflectivity curve is a superposition of slightly different curves stemming from slightly different interfacial structures. Thus the data are difficult to describe by a simple layer model.

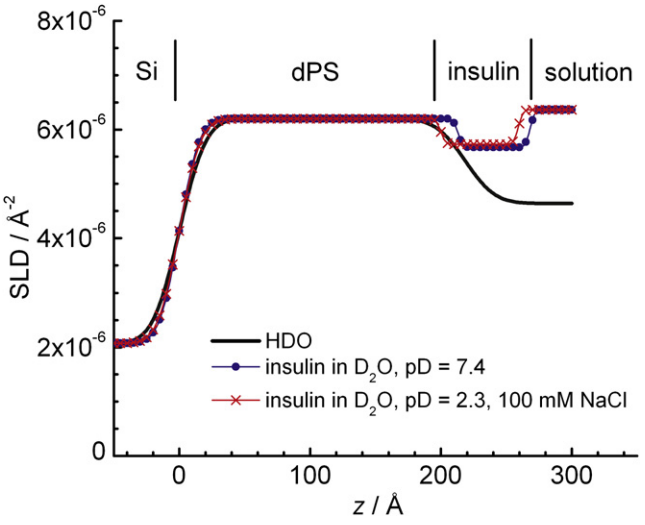

FIGURE 6 Scattering-length density (SLD) profiles of a silicon-dPS-solution interface without and with adsorbed insulin (20°C), as derived from neutron reflectivity curves. Thick solid curve was obtained with a 3:1 D_2O/H_2O mixture (denoted as HDO) in the absence of insulin. Thin solid lines with symbols reflect interfacial structures when the solution contains insulin in D_2O. In the latter case, an insulin adsorbate forms on the dPS surface.

An additional neutron reflectivity curve was measured after exchanging the sample solution with an insulin solution in D_2O at pD 2.3, containing 100 mM NaCl (data not shown). By lowering the pD value of the solution, insulin oligomers formed at pD 7.4 dissociate to form predominantly dimers (10,37). As a result of this dissociation, insulin can penetrate deeper into the rough dPS surface at pD 2.3 than at pD 7.4, as clearly reflected in the measured scattering-length density profile (Fig. 6). However, no change in the total mass of adsorbed insulin can be detected by lowering the pD value. Finally, the sample cell was heated to 60°C (where insulin is known to aggregate in solution), but this heat treatment did not result in a significant change of interfacial structure (Table 1).

Electrostatic driving forces for insulin adsorption at an interface were probed by the preparation of the polyelectrolyte multilayer structures Si-PEI-PSS-$(PAH-PSS)_4$-PAH and Si-PEI-PSS-$(PAH-PSS)_5$. These structures end with a positively charged PAH and a negatively charged PSS. Because the polyelectrolytes used were not deuterated, their structures (thickness, scattering-length density, and roughness) were determined from neutron reflectivity curves taken with D_2O-buffer solution, which generates a large contrast. The neutron reflectivity curves were fitted on the basis of a one-layer model Si/multilayer/solution (Table 1), and the scattering-length density profiles obtained are shown in Fig. 7. Then, by filling the sample cell with insulin solution, insulin adsorbs on the polyelectrolyte multilayers. After 1 h of incubation, neutron reflectivity curves were measured, as shown in Fig. 5. Unlike IAPP, insulin adsorbates on a polyelectrolyte multilayer are thick enough to analyze the neutron reflectivity curves on the basis of a two-layer model, Si/multilayer/insulin adsorbate/insulin solution (Table 1). The

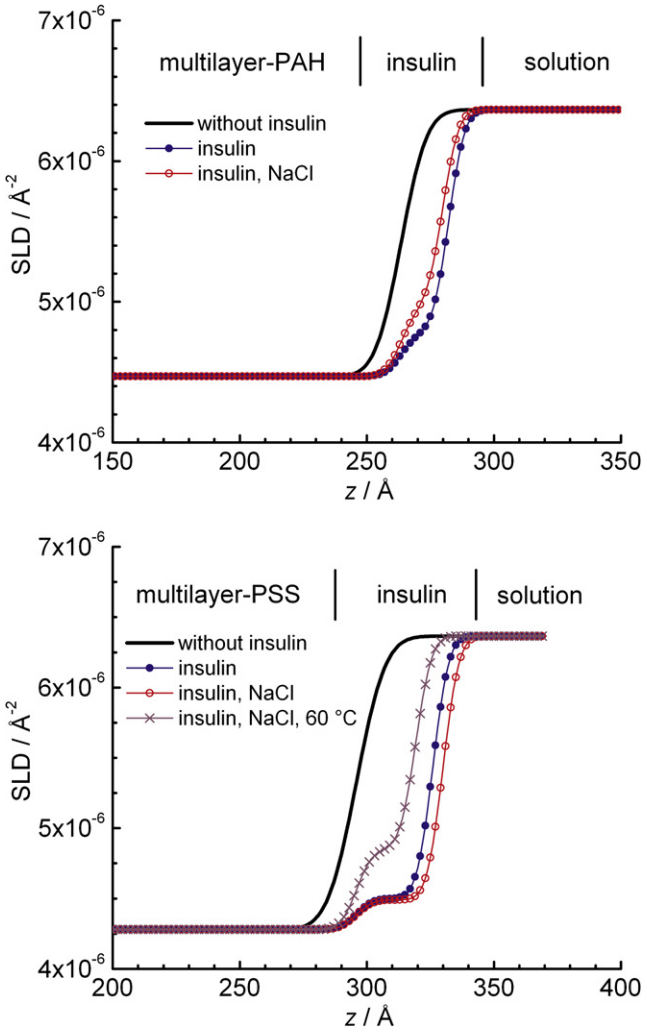

FIGURE 7 Scattering-length density (SLD) profiles of silicon-polyelectrolyte multilayer-solution interfaces. Thick solid curves indicate interfacial structures in the absence of insulin. Thin solid curves with symbols reflect interfacial structures when the solution contains insulin, and insulin adsorbates form on multilayers (20°C, pD 7.4). Silicon surface is located at $z = 0$ Å.

scattering-length density profiles obtained in this way are also plotted in Fig. 7.

As seen in Fig. 7, a much thicker insulin adsorbate forms on a PSS surface than on a PAH surface. Using a 0.1 mg mL^{-1} (17 μM) insulin solution (pD 7.4, 20°C), a 19-Å-thick adsorbate with an insulin volume fraction of 0.51 is found on PAH, whereas on PSS, the adsorbate is 30 Å thick, with a volume fraction of 0.60. These structural parameters lead to adsorbed amounts of 1.3 mg m^{-2} on PAH, and 2.5 mg m^{-2} on PSS (Eq. 2). It may be surprising that significantly more insulin is adsorbed on the negatively charged PSS surface, insofar as insulin has a negative net charge at pD 7.4. However, this finding is consistent with an insulin aggregation study performed earlier on lipid membranes (18). In that study, adding negatively charged lipid molecules to a lipid membrane led to an acceleration of the formation of insulin amyloid fibrils. The negatively charged lipids likely accumulate insulin molecules on the membrane surface, so that nucleus formation is highly facilitated.

So far, no clear explanation can be given as to why insulin prefers to adsorb at a negatively charged PSS surface at pD 7.4, compared with a positively charged PAH surface. Generally, close to the isoelectric point of insulin at pH 5.3 (19), the net charge of insulin may play a secondary role in the interaction with a charged surface. Rather, the distribution of positive and negative charges on a protein surface may be of primary importance. In this way, the negative charges of insulin stemming from four glutamic-acid residues may be less accessible and cannot easily come into contact with a surface. Furthermore, insulin has an inherent tendency to self-associate at pH 7 (38,39), which modulates the number and type of accessible surface charges in a complicated way.

However, on the addition of 100 mM NaCl to the insulin solution, the degree of insulin adsorption on the polyelectrolyte multilayers changes in a way that reflects the net charge of insulin molecules at pD 7.4. On a PAH surface, the added salt screens the net electrostatic attraction between the protein and the interface, resulting in a thinner adsorbate (Fig. 7) and a loss of adsorbed insulin from 1.3 to 1.0 mg m^{-2}. Likewise, at a PSS surface, the insulin adsorbate grows in thickness upon adding salt (Fig. 7), because of the screening of a net electrostatic repulsion. At the same time, the adsorbed mass of insulin increases from 2.5 to 2.9 mg m^{-2}.

Finally, an interesting result was obtained after heating the sample with insulin adsorbed on a PSS surface from 20°C to 60°C. As seen in the corresponding scattering-length density profile shown in Fig. 7, insulin desorbs partially by this heat treatment. About 1.6 mg m^{-2} of insulin remained adsorbed at 60°C. This heat-induced desorption may reflect an exothermic driving force for insulin adsorption on a PSS surface. This driving force may be the electrostatic attraction between local positive charges of insulin and the negative charges of PSS. Unfortunately, no heating was possible when PAH formed the outer layer. It was found repeatedly that the multilayer Si-PEI-PSS-(PAH-PSS)$_4$-PAH (with an odd number of layers) disintegrates in contact with D_2O buffer solution at 60°C. This finding is consistent with the odd-even effect reported in the literature for polyelectrolyte multilayers. For example, when a PAH-PSS multilayer is built up, the solvent fraction of the multilayer alternates for each additional layer (40). In addition, capsules made of poly-(diallyldimethylammonium chloride)-PSS multilayers break at 60°C, when the number of layers is odd, but are stable up to 90°C otherwise (41).

CONCLUSIONS

To summarize the main results of this study, the adsorbed amounts of IAPP and insulin at different polymer surfaces under various conditions are listed in Table 1. Regarding

IAPP, which carries 3–4 positive charges at pD 7.4, the strongest adsorption was evident at a hydrophobic interface. In proceeding from the hydrophobic dPS surface to the hydrophilic, negatively charged PSS surface, the adsorbed amount was reduced by ~50%. Almost all IAPP desorbs from PSS when adding salt to the IAPP solution. At the hydrophilic, positively charged PAH surface, almost no IAPP can be detected. On the basis of these findings, one may speculate that IAPP binds to a lipid membrane essentially via hydrophobic interactions with the lipid chains. This implies a partial insertion of the peptide into the membrane, as found in other studies (6–8). Attractive electrostatic interactions between negatively charged lipid headgroups and IAPP are unlikely to warrant the permanent lipid membrane binding of IAPP, in particular at slightly elevated ionic strength. However, interactions of IAPP with lipid headgroups via charges might lower the energy barrier for partitioning, i.e., for separating lipid molecules and inserting between the lipid chains. On the other hand, insulin most strongly adsorbs at a hydrophilic, negatively charged PSS surface at pD 7.4, although it has a small negative net charge at neutral pD values. This result might indicate a favorable interaction of insulin with negatively charged lipids. This conclusion could explain why the presence of DOPS in a lipid membrane accelerates the formation of insulin amyloid fibrils (18). A preferred localization and accumulation of insulin at this lipid will help form a nucleus for fibril growth.

This study was supported by the Deutsche Forschungsgemeinschaft and the Helmholtz-Zentrum Berlin.

REFERENCES

1. Westermark, P. 2005. Aspects on human amyloid forms and their fibril polypeptides. *FEBS J.* 272:5942–5949.
2. Jayasinghe, S. A., and R. Langen. 2007. Membrane interaction of islet amyloid polypeptide. *Biochim. Biophys. Acta.* 1768:2002–2009.
3. Knight, J. D., and A. D. Miranker. 2004. Phospholipid catalysis of diabetic amyloid assembly. *J. Mol. Biol.* 341:1175–1187.
4. Sparr, E., M. F. M. Engel, D. V. Sakharov, M. Sprong, J. Jacobs, et al. 2004. Islet amyloid polypeptide-induced membrane leakage involves uptake of lipids by forming amyloid fibers. *FEBS Lett.* 577:117–120.
5. Brender, J. R., E. L. Lee, M. A. Cavitt, A. Gafni, D. G. Steel, et al. 2008. Amyloid fiber formation and membrane disruption are separate processes localized in two distinct regions of IAPP, the type-2-diabetes-related peptide. *J. Am. Chem. Soc.* 130:6424–6429.
6. Engel, M. F. M., H. A. Yigittop, R. C. Elgersma, D. T. S. Rijkers, R. M. J. Liskamp, et al. 2006. Islet amyloid polypeptide inserts into phospholipid monolayers as monomer. *J. Mol. Biol.* 356:783–789.
7. Balali-Mood, K., R. H. Ashley, T. Hauß, and J. P. Bradshaw. 2005. Neutron diffraction reveals sequence-specific membrane insertion of pre-fibrillar islet amyloid polypeptide and inhibition by rifampicin. *FEBS Lett.* 579:1143–1148.
8. Lopes, D. H. J., A. Meister, A. Gohlke, A. Hauser, A. Blume, et al. 2007. Mechanism of islet amyloid polypeptide fibrillation at lipid interfaces studied by infrared reflection absorption spectroscopy. *Biophys. J.* 93:3132–3141.
9. Larson, J. L., and A. D. Miranker. 2004. The mechanism of insulin action on islet amyloid polypeptide fiber formation. *J. Mol. Biol.* 335:221–231.
10. Brange, J., L. Andersen, E. D. Laursen, G. Meyn, and E. Rasmussen. 1997. Toward understanding insulin fibrillation. *J. Pharm. Sci.* 86:517–525.
11. Jiménez, J. L., E. J. Nettleton, M. Bouchard, C. V. Robinson, C. M. Dobson, et al. 2002. The protofilament structure of insulin amyloid fibrils. *Proc. Natl. Acad. Sci. USA.* 99:9196–9201.
12. Sluzky, V., J. A. Tamada, A. M. Klibanov, and R. Langer. 1991. Kinetics of insulin aggregation in aqueous solutions upon agitation in the presence of hydrophobic surfaces. *Proc. Natl. Acad. Sci. USA.* 88:9377–9381.
13. Nielsen, L., R. Khurana, A. Coats, S. Frokjaer, J. Brange, et al. 2001. Effect of environmental factors on the kinetics of insulin fibril formation: elucidation of the molecular mechanism. *Biochemistry.* 40:6036–6046.
14. Smirnovas, V., and R. Winter. 2008. Revealing different aggregation pathways of amyloidogenic proteins by ultrasound velocimetry. *Biophys. J.* 94:3241–3246.
15. Dzwolak, W., S. Grudzielanek, V. Smirnovas, R. Ravindra, C. Nicolini, et al. 2005. Ethanol-perturbed amyloidogenic self-assembly of insulin: looking for origins of amyloid strains. *Biochemistry.* 44:8948–8958.
16. Dzwolak, W., V. Smirnovas, R. Jansen, and R. Winter. 2004. Insulin forms amyloid in a strain-dependent manner: an FT-IR spectroscopic study. *Protein Sci.* 13:1927–1932.
17. Hong, D. -P., and A. L. Fink. 2005. Independent heterologous fibrillation of insulin and its B-chain peptide. *Biochemistry.* 44:16701–16709.
18. Grudzielanek, S., V. Smirnovas, and R. Winter. 2007. The effects of various membrane physical-chemical properties on the aggregation kinetics of insulin. *Chem. Phys. Lipids.* 149:28–39.
19. Wintersteiner, O., and H. A. Abramson. 1933. The isoelectric point of insulin. *J. Biol. Chem.* 99:741–753.
20. Baszkin A. and Norde W., editors. (2000). Physical Chemistry of Biological Interfaces. Marcel Dekker, New York.
21. Russell, T. P. 1990. X-ray and neutron reflectivity for the investigation of polymers. *Mater. Sci. Rep.* 5:171–271.
22. Hollmann, O., R. Steitz, and C. Czeslik. 2008. Structure and dynamics of α-lactalbumin adsorbed at a charged brush interface. *Phys. Chem. Chem. Phys.* 10:1448–1456.
23. Jackler, G., C. Czeslik, R. Steitz, and C. A. Royer. 2005. Spatial distribution of protein molecules adsorbed at a polyelectrolyte multilayer. *Phys. Rev. E Stat. Nonlin. Soft Matter Phys.* 71, 041912.
24. Rocha, S., R. Krastev, A. F. Thünemann, M. C. Pereira, H. Möhwald, et al. 2005. Adsorption of amyloid β-peptide at polymer surfaces: a neutron reflectivity study. *ChemPhysChem.* 6:2527–2534.
25. Covington, A. K., M. Paabo, R. A. Robinson, and R. G. Bates. 1968. Use of the glass electrode in deuterium oxide and the relation between the standardized pD (pa_D) scale and the operational pH in heavy water. *Anal. Chem.* 40:700–706.
26. Kern, W. 1990. The evolution of silicon wafer cleaning technology. *J. Electrochem. Soc.* 137:1887–1892.
27. Decher, G. 1997. Fuzzy nanoassemblies: toward layered polymeric multicomposites. *Science.* 277:1232–1237.
28. Mezei, F., R. Golub, F. Klose, and H. Toews. 1995. Focussed beam reflector for solid and liquid surfaces. *Physica B.* 213 and 214: 898–900.
29. National Institute of Standards and Technology. Neutron scattering length and cross sections. http://www.ncnr.nist.gov/resources/n-lengths/list.html. Accessed April 2008.
30. Steitz, R., T. Gutberlet, T. Hauss, B. Klösgen, R. Krastev, et al. 2003. Nanobubbles and their precursor layer at the interface of water against a hydrophobic substrate. *Langmuir.* 19:2409–2418.
31. Cooper, G. J. S., A. J. Day, A. C. Willis, A. N. Roberts, K. B. M. Reid, et al. 1989. Amylin and the amylin gene: structure, function and relationship to islet amyloid and to diabetes mellitus. *Biochim. Biophys. Acta.* 1014:247–258.
32. Jackler, G., R. Steitz, and C. Czeslik. 2002. Effect of temperature on the adsorption of lysozyme at the silica/water interface studied by optical and neutron reflectometry. *Langmuir.* 18:6565–6570.

33. Koo, J., T. Gutberlet, and C. Czeslik. 2008. Control of protein interfacial affinity by nonionic cosolvents. *J. Phys. Chem. B*. 112:6292–6295.

34. Jayasinghe, S. A., and R. Langen. 2005. Lipid membranes modulate the structure of islet amyloid polypeptide. *Biochemistry*. 44:12113–12119.

35. Smith, L. F. 1966. Species variation in the amino acid sequence of insulin. *Am. J. Med*. 40:662–666.

36. Smirnovas, V., R. Winter, T. Funck, and W. Dzwolak. 2006. Protein amyloidogenesis in the context of volume fluctuations: a case study on insulin. *ChemPhysChem*. 7:1046–1049.

37. Whittingham, J. L., D. J. Scott, K. Chance, A. Wilson, J. Finch, et al. 2002. Insulin at pH 2: structural analysis of the conditions promoting insulin fibre formation. *J. Mol. Biol*. 318:479–490.

38. Jeffrey, P. D., B. K. Milthorpe, and L. W. Nichol. 1976. Polymerization pattern of insulin at pH 7.0. *Biochemistry*. 15:4660–4665.

39. Pocker, Y., and S. B. Biswas. 1981. Self-association of insulin and the role of hydrophobic bonding: a thermodynamic model of insulin dimerization. *Biochemistry*. 20:4354–4361.

40. Carrière, D., R. Krastev, and M. Schönhoff. 2004. Oscillations in solvent fraction of polyelectrolyte multilayers driven by the charge of the terminating layer. *Langmuir*. 20:11465–11472.

41. Köhler, K., D. G. Shchukin, H. Möhwald, and G. B. Sukhorukov. 2005. Thermal behavior of polyelectrolyte multilayer microcapsules. 1. the effect of odd and even layer number. *J. Phys. Chem. B*. 109: 18250–18259.